ADVANCED FUNCTIONAL MATERIALS

Morphology-Controlled Growth of Large-Area Two-Dimensional Ordered Pore Arrays**

By *Fengqiang Sun*, *Weiping Cai*,* *Yue Li*, *Bingqiang Cao*, *Yong Lei*, and *Lide Zhang*

A solution-dipping template strategy for large-area synthesis of morphology-controlled, ordered pore arrays is reported. The morphology of the pore array can easily be controlled by concentration of the precursor solution and treatment conditions. With decrease of the concentration from a high level to a very low level nanostructured complex (pore–hole, and pore–particle) arrays, through-pore arrays, and even ring arrays can, in turn, be obtained. The pore size is adjustable over a large range by changing the diameter of the template's latex spheres. This synthesis route is universal and can be used for various metals, semiconductors and compounds on any substrate. Such structures may be useful in applications such as energy storage or conversion, especially in integrated next-generation nanophotonics devices, and biomolecular labeling and identification.

1. Introduction

Two-dimensional (2D) ordered pore arrays (films) have a high specific surface area and an orderly arrangement of pores, and they play an important role in many applications, such as catalysis,[1] gas sensors,[2] photonic[3] and opto-electronic devices,[4] surface-enhanced Raman scattering (SERS),[5] thermal insulation materials,[6] and membranes.[7] The type of material and its pore morphology is usually determined by the desired application. In general, ordered pore arrays can be synthesized by electron-beam lithography,[8] microcontact printing,[9] and self-assembly techniques,[10,11] etc. Recently, the use of colloidal crystals as a template has shown great promise for the fabrication of three-dimensional (3D) highly ordered porous materials,[5,12–15] and also for 2D ordered pore arrays (films).[16] Based on 2D colloidal crystals of latex spheres, which can be easily synthesized by many methods such as drop-coating,[17] spin-coating,[18] or vertical withdrawing,[19] many researchers[20–23] have fabricated periodical particle arrays on a substrate by element deposition. Recently, various groups have reported ordered TiO_2 and gold porous films fabricated by spray pyrolysis,[1] sol–gel,[24] and colloidal suspension techniques.[5,25] Nevertheless, the morphology-controlled growth of large-area, ordered pore arrays remains a challenge, and receives a great deal of attention in the field of establishing parallel nanofabrication techniques.

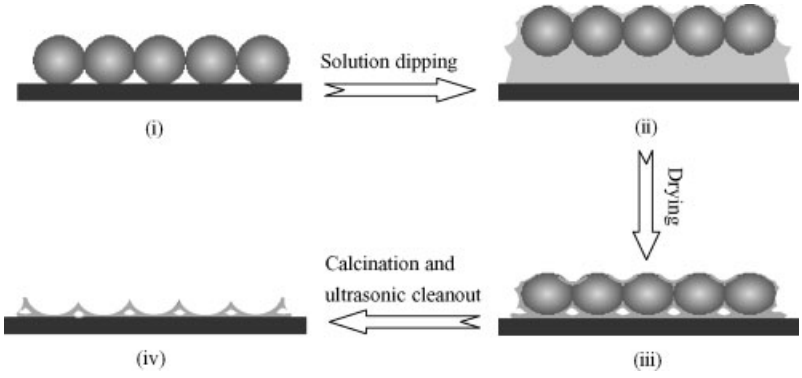

Figure 1. Schematic illustrations of the solution-dipping template strategy. i) Template (large-area monolayer colloidal crystal) on a substrate. ii) The colloidal crystal floats on the surface of the precursor solution. iii) Integrity of the solute and latex spheres. iv) Ordered porous film.

Here, we describe an alternative route, the solution-dipping template synthesis strategy shown in Figure 1, for the large-area synthesis of morphology-controlled ordered pore arrays, which can be used for various metals, semiconductors, and compounds on any substrate. As we confirmed experimentally, after dropping a precursor solution onto a substrate at the edge of a monolayer polystyrene colloidal crystal template with an area larger than 1 cm^2, the template will float due to the surface tension of the solution. Subsequent drying treatment, below the glass-transition temperature of polystyrene, will lead to deformation of the latex spheres, to a certain degree (depending on the drying temperature and time[26,27]), and solute precipitation or deposition on the surface of these deformed spheres and the substrate. After removal of the template (by calcination and/or ultrasonic vibration or dissolution), an ordered pore array can thus be obtained. The array morphologies can be easily controlled by the solution concentration and the sphere deformation during drying. Because the template floats on the solution, the pores could be upper-end open or two-end open (through-pores) depending on the solution concentration. It should be mentioned that the colloidal monolayer can also

[*] Prof. W. Cai, F. Sun, Y. Li, B. Cao, Prof. L. Zhang
Institute of Solid State Physics, Chinese Academy of Sciences
Hefei, 230031, Anhui (China)
E-mail: wpcai@issp.ac.cn
Dr. Y. Lei
Singapore-MIT Alliance, National University of Singapore
04-10, 4 Engineering Drive 3, 117576, Singapore.

[**] This study was co-supported by the National Natural Science Foundation of China (Grant number: 50271069), and National "973" Project of China (Grant No: G1999064501)

 DOI: 10.1002/adfm.200305055

be transferred onto any substrate.[28] We can thus structure pore arrays with controllable morphologies on a desired substrate.

Taking Fe_2O_3 as an example, which is one type of functional material that has been widely studied in powders,[29] Fe_2O_3/SiO_2 composites,[30] granular films,[31] Fe_2O_3/mesporous aluminosilicates,[32] particle arrays,[33] and 3D porous structures,[34] we show here that a large area, ordered pore array with a controllable morphology can be formed on any desired substrate by the strategy presented in this article.

2. Results and Discussion

Figure 2 shows some results for samples (on a glass substrate), with different precursor concentrations, dried in an oven at 80 °C for two hours and then heated at 400 °C for eight hours, followed by ultrasonic cleanout (0.5 h). A series of pore arrays with different morphologies was obtained. X-ray diffraction (XRD) confirmed that the porous films consist of crystalline α-Fe_2O_3 (data not shown here). When the concentration is 0.02 M or higher, honeycomb structures are always formed, excepting the pore shapes and diameters at the film surface, which depend on the precursor concentrations. A high concentration (0.8 M) gives rise to pores with nearly circular upper-end openings. The diameter of the openings at the film surface is obviously smaller than that of the polystyrene sphere (PS) (Fig. 2A). There is a small triangular hole at the interstitial position of the closely packed PSs and nanogaps on some pore walls (skeletons). The porous structure is more clearly revealed by tilted views. The porous film is actually a nearly spherical hollow array with truncated tops as openings. The bottom of the spherical hollow is buried in the α-Fe_2O_3 film, as illustrated in Figure 3A, which was taken at the edge region of the film. In addition, there are holes in the pore walls between two adjacent pores (inset of Fig. 3A). As the precursor concentration decreases, the truncated shape of the pores at the film surface gradually becomes a regular hexagon (Figs. 2B,C). The distance between the opposite sides of the hexagon is close to the diameter of the PSs. In addition, a clear triangular (for the 0.08 M solution) or spherical (for the 0.06 M solution) particle appears at the interstitial positions of the closely packed three spheres or nodes of the skeleton network, instead of a hole; no gaps were observed in the pore walls. When the precursor con-

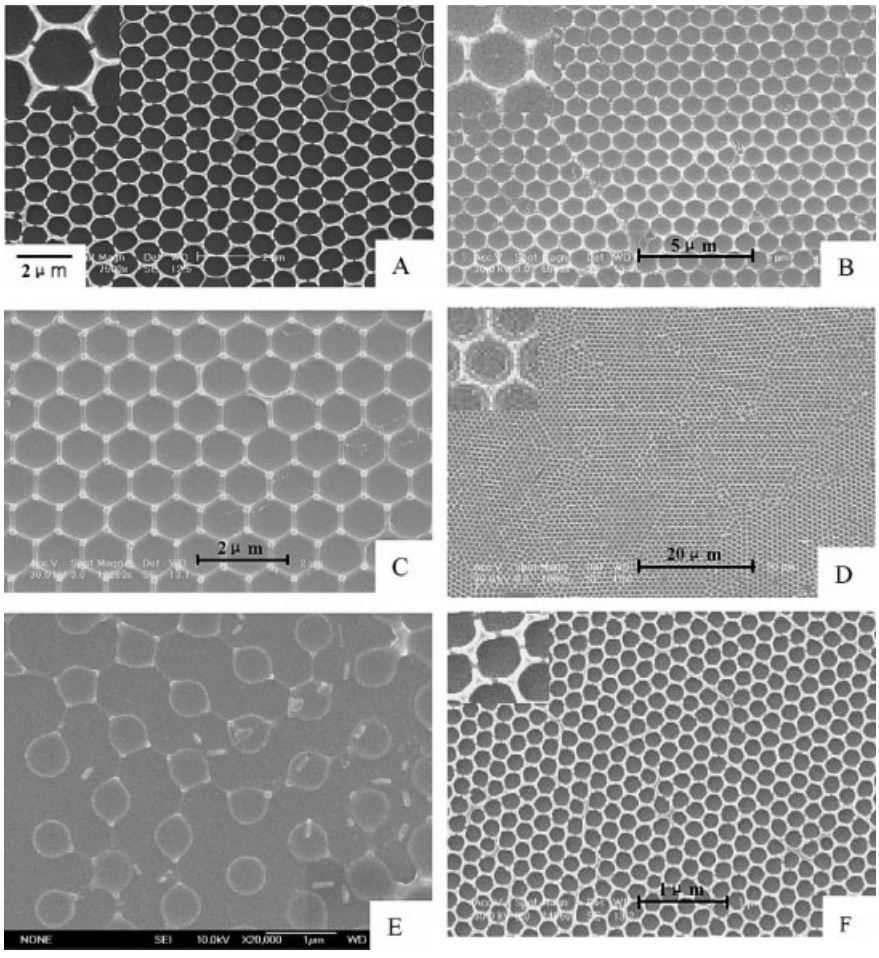

Figure 2. Field-emission SEM topographic images for samples with different concentrations of precursor solutions, dried at 80 °C (2 h) and subsequently calcinated at 400 °C (8 h), followed by ultrasonic cleanout (0.5 h). A) 0.8 M. B) 0.08 M. C) 0.06 M. D) 0.02 M. E) 0.002 M. F) 0.8 M. (A)–(E) correspond to the template with 1000 nm PSs, and (F) corresponds to the template with 200 nm PSs.

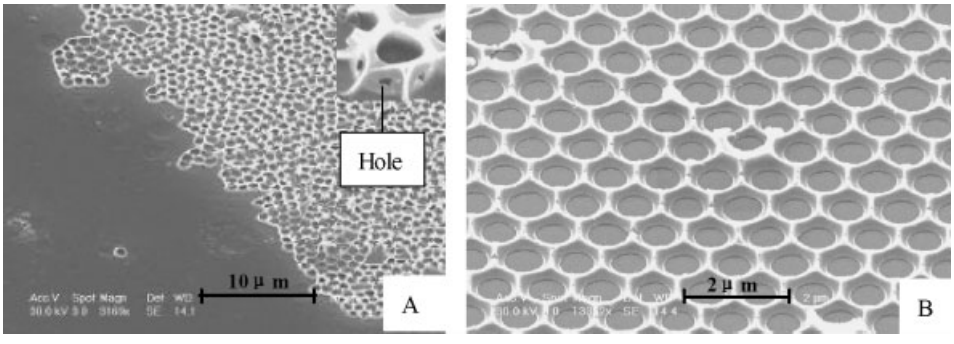

Figure 3. Tilt views of ordered porous films. A) The sample corresponding to Figure 2A (in the edge region of the film). B) The sample corresponding to Figure 2D.

ADVANCED FUNCTIONAL MATERIALS

centration is reduced to 0.02 M, a through-pore structured film (with two open-ended pores) is formed (Fig. 2D). This is seen more clearly in a tilt view, as shown in Figure 3B,[35] where we can see that the pore diameters at the bottom (circular) and top (hexagonal) of the pore are different, at about 500 and 1000 nm respectively. The pores in the samples above are all ordered and closely arranged, bounded with the inter-connected net-like skeletons. However, as the concentration is reduced to a very low level (0.002 M), a ring array, rather than the closely arranged pore array, is formed (Fig. 2E). Most of these rings are not perfectly circular. All the rings surround the positions where the latex spheres were originally located on the substrate and hence they are also arranged in hexagons. Further experiments revealed that the size of the PSs does not significantly influence the morphology of the pore array. Figure 2F shows a typical result. When a precursor solution with a concentration of 0.8 M is applied onto the template with much smaller PSs (200 nm), the morphology of the porous film is similar to Figure 2A, except for the pore size. It should be mentioned that the center-to-center distance between adjacent pores or rings is always close to the diameter of the PSs, irrespective of the solution concentration.

Now let us briefly discuss the formation of pore arrays with different morphologies. Changes in the shape of the PSs during evaporation are essential to the morphologies. However, subsequent treatments are also important. When the colloidal monolayer template is dropped with the precursor solution, it floats on top of the solution. The interstitial spaces of the closely packed PSs are then filled with the solution due to capillary action, and a meniscus is formed on the solution surface, as illustrated schematically in Figure 4A. During subsequent drying at 80 °C, the liquid surface and the colloidal monolayer gradually decrease due to evaporation of solvent, thereby deforming the PSs. When the concentration of the solution reaches the saturation point further drying will lead to solute precipitation on the spheres' surface and the substrate. Finally, a nearly triangular hole is left between two adjacent spheres and the substrate due to lack of sufficient solution compensation (Figs. 4B–E), similar to the pore-formation mechanism in metal casting.[36] Obviously, the lower the solution concentration, the longer the time to reach saturation induced by evaporation at the same drying temperature, leading to a more obvious change in sphere shape.

For the sample with a high concentration (0.8 M) of precursor, the above-mentioned process is finished in a shorter time. Therefore, the latex spheres only undergo a small deformation before complete evaporation,[37] and there is only a small contact area between two adjacent PSs, which leads to the formation of small circular holes in the pore walls (inset in Figs. 3A,4B). Subsequent calcination and ultrasonic cleanout destroy some of the holes and hence form the nanogaps in the pore walls, as shown in Figure 2A. Because the pore walls above the tangent-point plane of PSs (Fig. 4A) were not removed, triangular holes can be observed, in the top view, at the interstitial positions of the closely packed three spheres, or nodes of the skeleton network, and the pore size at the film surface is smaller than the diameter of the latex spheres.

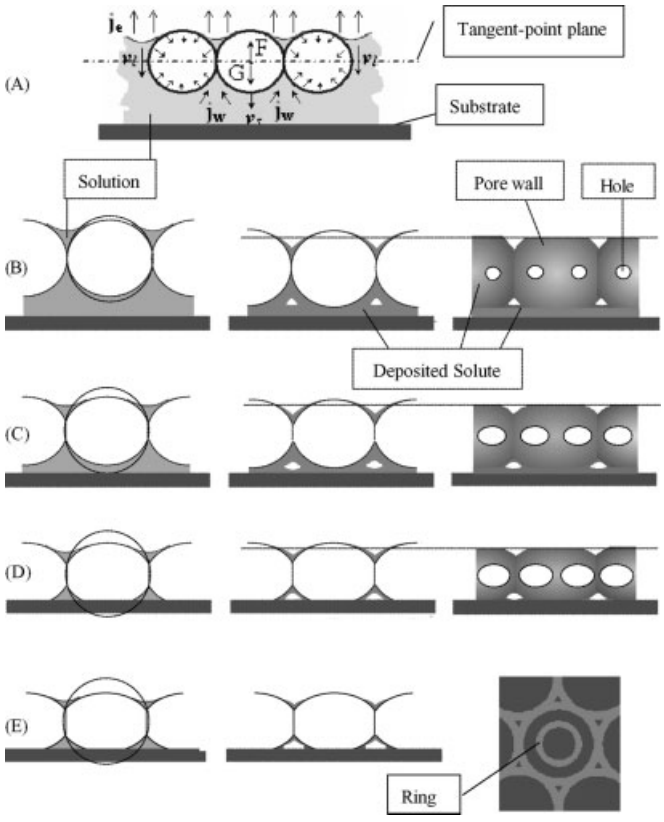

Figure 4. Schematic illustrations of the formation process of ordered porous films for different concentrations of precursor solutions. A) Latex spheres are floating on the solution. F and G denote the flotage and gravitation of the polystyrene spheres respectively. J_e is the water evaporation flux, J_w the water influx, ν_l and ν_s are the descending rate of the solution surface and the colloid crystal, respectively. B) High concentration (0.8 M). C) 0.08 M and 0.06 M. D) Low concentration (0.02 M). E) Very low concentration (0.002 M). Left column: the solutions reach saturation. Middle column: complete evaporation of solvent. Right column: after removal of the template by dissolution. The illustration for (E) in this column is a top view.

When the solution concentration is lowered (to 0.08 M and 0.06 M), it takes a longer time for the solution to become saturated, leading either to a larger contact area between two adjacent spheres (Fig. 4C) or larger holes in the pore wall due to deformation of the spheres. After removal of the spheres by calcination and ultrasonic cleanout, the solute deposited on the sphere surface above the tangent-point plane will be removed because the holes in the pore wall are too big, but triangular [for the sample with higher precursor concentration (0.08 M)] or nearly spherical [for that with smaller one (0.06 M)] offshoots are left on the nodes of the skeleton network due to the template geometry (Figs. 2B,C). The large contact area between two adjacent spheres originating from their deformation during drying leads to the formation of hexagonal openings at the film surface.

If the solution concentration is decreased further (to 0.02 M), before solution saturation and solute precipitation, the latex spheres have already come into contact with the substrate, and this contact area has become large enough due to

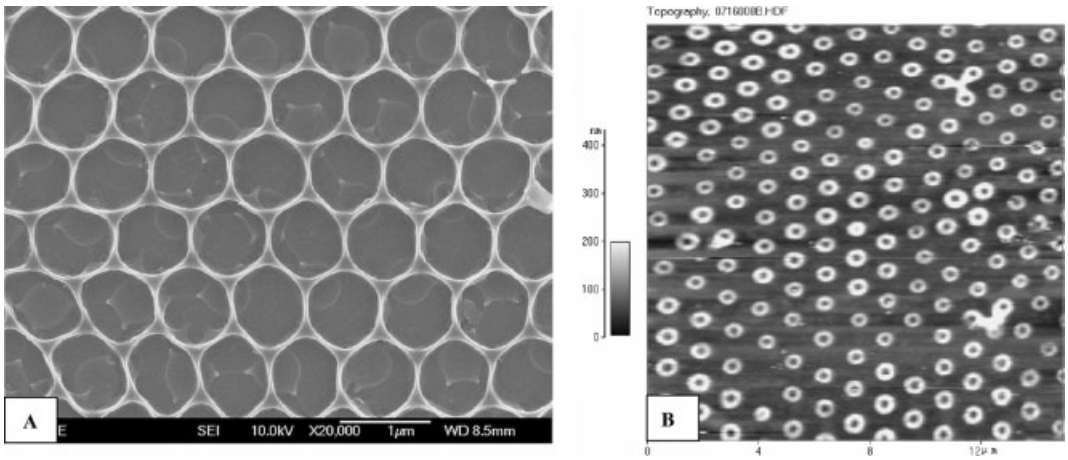

Figure 5. The sample from 0.002 M solution after drying at 80 °C (2 h). A) After subsequent heating at 400 °C (8 h) and ultrasonic vibration for a few minutes (instead of 0.5 h). B) After subsequent ultrasonic washing in dichloromethane solution for 0.5 h.

their deformation during drying (as illustrated in Fig. 4D), pores with two-ended openings are formed (Figs. 2D,3B).

For the same reason, when the concentration of the precursor is reduced to a very low level (0.002 M), only a thin solute deposition (shell) is preferentially formed on the free surface of the latex spheres above and below the tangent-point plane (Fig. 4E). Subsequent calcination at 400 °C (8 h) and then ultrasonic vibration for a short time (a few minutes) removes the latex spheres but leaves the deposited shell, as shown in Figure 5A. There are two layers, and the top layer is slightly displaced with respect to the bottom layer due to ultrasonic vibration. However, we can still see some irregular rings in the bottom layer. After ultrasonically washing for an additional half hour, the top layer is removed and the bottom layer, a ring array, can be seen (see Fig. 2E). Further experiments indicate that the non-circular shape of the rings results from calcination at 400 °C after drying at 80 °C. Ultrasonically washing the sample in dichloromethane solution after drying at 80 °C, without calcination, gives an array of circular rings (Fig. 5B).

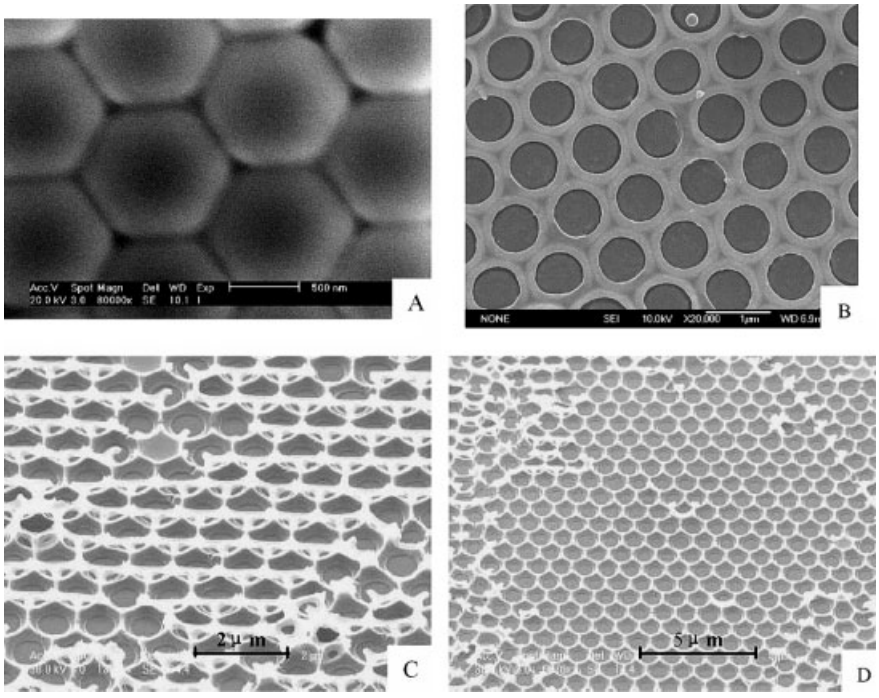

Figure 6. Typical transitional states during porous film formation for the sample from 0.02 M precursor solution. A) After solution-dipping and drying at 80 °C for 2 h. B) After dissolution in dichloromethane for sample (A). C) After calcination at 400 °C (8 h) for sample (A). D) After ultrasonic vibration for a few minutes for sample (C).

Based on the discussions above, there should be some intermediate states during the formation of the pores. Figure 6 shows such changes of the sample with a 0.02 M precursor solution. After drying the solution-dipped sample at 80 °C for two hours, the PSs have been deformed (Fig. 6A). The spheres have become concave on top and are nearly hexagonal, with greatly increased contact between neighboring spheres, which shows that they had been sintered to a certain degree. If we put such a sample into dichloromethane to dissolve the spheres, instead of burning them away, and then perform an ultrasonic cleanout, a circular open array (as seen from the top view) is left (Fig. 6B). The diameter of the openings is smaller than that of the latex spheres, which is similar to the final structure of the sample from 0.8 M solutions (Fig. 2A). Further experiments revealed that there is a solute-deposition shell on the sphere surface above the tangent-point plane in all samples, irrespective of the solution concentrations. Therefore, the final

ADVANCED FUNCTIONAL MATERIALS

structure and morphology of the ordered pore array also depend on the subsequent template-removal method—burning, ultrasonic vibration, or dissolution—in addition to the concentration of the solution. Upon calcining the sample shown in Figure 6A, we can see a two-layer porous structure (Fig. 6C). The two layers are connected at the nodes of the skeleton network in the bottom layer. Subsequent ultrasonic washing for a few minutes removes the whole top layer almost completely, as shown in Figure 6D. Further ultrasonic vibration leads to the final structure in Figure 3B.

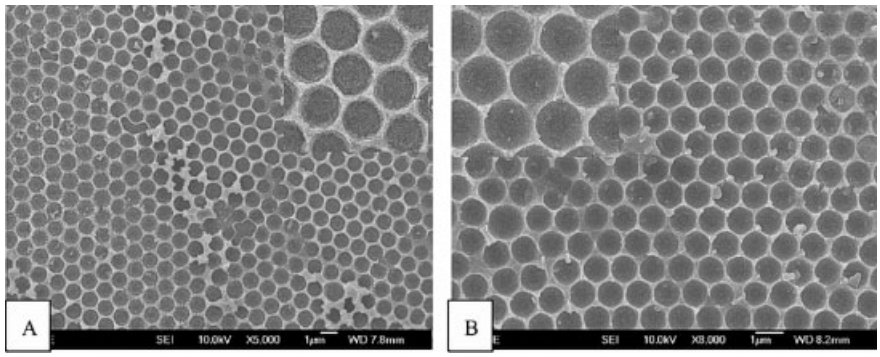

Figure 7. Through-pore structures of zinc (A) and CeO_2 (B) on silicon substrate with the solution-dipping template strategy. Treatment conditions: A) Precursor—$Zn(OOCCH_3)_2$ (0.1 M), 80 °C for 2 h and 200 °C for 8 h in air, and 350 °C for 4 h under H_2 followed by ultrasonic cleanout for 0.5 h; B) Precursor—$Ce(NO_3)_3$ (0.05 M), 80 °C for 2 h, and 200 °C for 8 h followed by ultrasonic cleanout for 0.5 h.

3. Conclusions

In summary, various ordered pore structured Fe_2O_3 films have been obtained using our solution-dipping template strategy. The porous film morphologies can be easily controlled by changing the concentration of the precursor solution and/or the treatment conditions. With a decrease of the concentration from a high to a very low level, nanostructured complex (pore-hole, and pore–particle) arrays, through-pore arrays and even ring arrays can be attained. We can also control the pore size over a large range by changing the diameter of the template's latex spheres. The synthesis strategy presented here is universal and can be used for other metal or oxide ordered pore arrays. We have synthesized a series of other morphology-controlled ordered porous films, such as zinc, ZnO, NiO, Co_2O_3, CuO, CeO_2, Eu_2O_3, and Dy_2O_3, with different concentration precursor solutions, and also fabricated these structures on other substrates by transferring the colloidal monolayer from one substrate to a desired substrate before the precursor solution is dipped. Figure 7 shows the through-pore structures of Zn and CeO_2 films on a silicon substrate. These morphology-controlled films will show controllable and enhanced optical properties, gas-sensing properties, catalyzing properties, and so on. Such structures may be useful in applications for energy storage or conversion, especially in next-generation integrated nanophotonics devices and biomolecular labeling and identification.

4. Experimental

The polystyrene sphere suspensions were bought from Alfa Aesar Corporation. The glass substrates were washed for around 10 min in ethanol and distilled water in an ultrasonic bath, and then they were sequentially cleaned according to Haynes et al. [38]. A 1 cm × 1 cm monolayer colloidal crystal was synthesized on the substrate by spin-coating in a custom-built spin-coater. This crystal can be transferred to any desired substrate, as illustrated in Figure 8 (from a glass to a silicon substrate). $Fe(NO_3)_3$ solutions with different concentrations were prepared from $Fe(NO_3)_3{\cdot}9H_2O$ dissolved in distilled water. A drop of the solution was applied onto the substrate at the edge of the colloid monolayer with a quantitative pipette, whereupon the monolayer floated on the surface of the solution. The sample was then placed into an oven horizontally and dried at 80 °C for two hours, followed by heating at 400 °C for eight hours to burn the latex spheres away and decompose the $Fe(NO_3)_3$ to Fe_2O_3. Finally, ultrasonic washing was performed for the calcined samples before sample characterization by scanning electron microscopy (SEM), atomic force microscopy (AFM), and XRD.

Received: September 24, 2003
Final version: November 14, 2003

A, B, C.

Figure 8. Photos depicting transferring a 1 cm × 1 cm monolayer colloidal crystal on glass substrate to silicon substrate. A) The monolayer on a glass substrate. B) Lift-off in water. C) Pick-up of the monolayer with an Si substrate.

[1] S. I. Matsushita, T. Miwa, D. A. Tryk, A. Fujishima, *Langmuir* **1998**, *14*, 6441.
[2] C. D. Elizabeth, K. V. Oomman, G. O. Keat, *Sensors* **2002**, *2*, 91.
[3] E. Yablonovitch, T. J. Gmitter, R. D. Meade, A. M. Rappe, *Phys. Rev. Lett.* **1991**, *67*, 80.
[4] M. Imada, S. Noda, A. Chutinan, T. Tokuda, *Appl. Phys. Lett.* **1999**, *75*, 316.
[5] P. M. Tessier, O. D. Velev, A. T. Kalambur, *Adv. Mater*. **2001**, *13*, 396.
[6] T. Bitzer, *Honeycomb Technology*, Chapman and Hall, London **1997**.
[7] R. E. Kesting, *Synthetic Polymer Membranes*, Wiley, New York **1985**.
[8] T. W. Ebbesen, H. J. Lezec, H. F. Ghaemi, *Nature* **1998**, *391*, 667.
[9] Y. Xia, J. Rogers, K. E. Paul, G. M. Whitesides, *Chem. Rev.* **1999**, *99*, 1823.
[10] M. H. Stenzel-Rosenbaum, T. P. Davis, A. G. Fane, *Angew. Chem. Int. Ed.* **2001**, *40*, 3428.
[11] P. S. Shah, M. B. Sigman, C. A. Stowell, *Adv. Mater.* **2003**, *15*, 971.
[12] S. M. Yang, N. Coombs, G. A. Ozin, *Adv. Mater*. **2000**, *12*, 1940.
[13] P. Jiang, J. F. Bertone, V. L. Colvin, *Science* **2001**, *291*, 453.
[14] D. Y. Wang, F. Caruso, *Adv. Mater*. **2003**, *15*, 205.
[15] H. Miguez, N. Tetreault, S. M. Yang, V. Kitaev, G. A. Ozin, *Adv. Mater*. **2003**, *15*, 597.
[16] X. Chen, Z. M. Chen, N. Fu, G. Lu, B. Yang, *Adv. Mater*. **2003**, *15*, 1413.
[17] R. Micheletto, H. Fukuda, M. Ohtsut. *Langmuir* **1996**, *11*, 3333.
[18] J. C. Hulteen, A. T. David, R. P. Van Duyne, *J. Phys. Chem. B* **1999**, *103*, 3854.
[19] A. S. Dimitrov, K. Nagayama, *Langmuir* **1996**, *12*, 1303.
[20] F. Burmeister, C. Schafle, P. Leiderer, *Adv. Mater.* **1998**, *10*, 495.
[21] C. L. Haynes, R. P. Van Duyne, *J. Phys. Chem. B* **2001**, *105*, 5599.
[22] C. W. Kuo, J. Y. Shiu, Y. H. Cho, P. Chen, *Adv. Mater.* **2003**, *15*, 1065.
[23] J. Rybczynski, U. Ebels, M. Giersig, *Colloids Surf., A* **2003**, *219*, 1.
[24] T. Tatsuma, A. Ikezawa, Y. Ohko, *Adv. Mater.* **2000**, *12*, 643.
[25] P. M. Tessier, O. D. Velev, A. T. Kalambur, *J. Am. Chem. Soc.* **2000**, *122*, 9554.
[26] S. Mazur, R. Beckerbauer, J. Buckholz. *Langmuir* **1997**, *13*, 4287.
[27] B. Gates, S. H. Park, Y. Xia. *Adv. Mater.* **2000**, *12*, 653.
[28] F. Burmeister, C .Schafle, P.Leiderer, *Langmuir* **1997**, *13*, 2983.
[29] F. S. Yen, W. C. Chen, J. M. Yang, *Nano Lett.* **2002**, *2*, 245.
[30] E. M. Moreno, M. ZaYat, M. P. Morales, *Langmuir* **2002**, *18*, 4972.
[31] L. H. Hou, W. Li, L.H. Lu, *Chem. Mater.* **2000**, *12*, 790.
[32] C. Garcia, Y. M. Zhang, F. DiSalvo, U. Wiesner, *Angew. Chem. Int. Ed.* **2003**, *42*, 1526
[33] Z. Y. Zhong, B. Gates, Y. N. Xia, *Langmuir* **2000**, *16*, 10 369.
[34] H. W. Yan, C. F. Blanford, B. T. Holland, *Chem. Mater.* **2000**, *12*, 1134.
[35] For the 0.08 M and 0.06 M samples, the pores are oblate hemispherical hollows with nearly or regularly hexagonal openings at the film surface, but are only open at the upper end.
[36] J. D. Verhoeven, *Fundamentals of Physical Metallurgy*, John Wiley and Sons, New York, **1975**.
[37] After solute deposition, the deformation of the PSs will be limited during further drying treatment due to the restriction of the deposited solute shell.
[38] C. L. Haynes, A. D. McFarland, M. T. Smith, *J. Phys. Chem. B* **2002**, *106*, 1898.

